

Light Scattering by Agglomerates: Coupled Electric and Magnetic Dipole Method

George W. Mulholland*

*Building and Fire Research Laboratory, National Institute of Standards and Technology,
Gaithersburg, Maryland 20899*

Craig F. Bohren

*Department of Meteorology, The Pennsylvania State University,
University Park, Pennsylvania 16802*

Kirk A. Fuller

Department of Atmospheric Science, Colorado State University, Fort Collins, Colorado 80523

Received October 22, 1993. In Final Form: May 19, 1994[®]

The coupled electric dipole method (CED) for treating light scattering by an agglomerate particle is extended to include both the electric and magnetic dipole terms (CEMD). The accuracy of these two methods along with the Rayleigh–Debye (RD) method is obtained by comparing with the exact solution for two spheres in contact. It is found that addition of the magnetic dipole term extends the range of the coupled dipole method from a primary sphere diameter of about 0.06 μm to about 0.12 μm for sootlike particles at visible wavelengths. The scattering and extinction cross sections, the differential scattering, and the polarization ratio are computed for agglomerates with 17, 52, and 165 primary spheres for sootlike and silica-like agglomerates. The agglomerates are generated by Brownian dynamics computer simulation of in-flame growth. A comparison is made among RD, CED, and CEMD. The effects of primary sphere diameter and agglomerate size on the validity of the RD approximation are discussed. It is shown that the polarization ratio computed by CEMD is sensitive to the primary sphere size independent of agglomerate size.

I. Introduction

Light scattering by agglomerates is of interest in two regards: scattering and absorption cross sections are of interest in their own right and structural information about agglomerates can be inferred from scattering measurements. The basic structural information includes the fractal dimension and the agglomerate size as characterized by the radius of gyration. The radius of gyration is determined from measurements of near-forward scattering whereas the fractal dimension is determined from measurements away from the forward direction.^{1,2} For absorbing agglomerates generated by computer simulation, Mountain and Mulholland (MM)³ demonstrated how the primary sphere size and number concentration of agglomerates could also be obtained from light scattering measurements together with light extinction measurements. Sorensen *et al.*⁴ used the MM approach to obtain the primary size of soot in a premixed methane–oxygen flame; Hall and Bonczyk⁵ also used the MM approach for a slot diffusion flame.

Recent interest in the optical properties of low density soot was motivated by concern about the climatic impact of global smoke clouds arising from a major nuclear war. The optical properties of soot were crucial to the analysis, yet there was no appropriate treatment of low density smoke agglomerates. Berry and Percival⁶ provided predictions of the cross sections as a function of agglomerate

size. Measurements by Colbeck *et al.*⁷ support some of the general features of the Berry–Percival theory but lack the detailed information on agglomerate structure needed for a quantitative assessment of this theory.

The analysis of Mountain and Mulholland³ is based on the Rayleigh–Debye scattering approximation in which each primary sphere acts as a dipole source of scattered radiation excited solely by the incident field. The Berry–Percival analysis adjusts the strength of the dipole based on a mean field estimate of the multiple scattering. Still, the results are identical to the Rayleigh–Debye theory within a multiplicative constant. Two conditions must be satisfied for the Rayleigh–Debye approximation to be valid. First the diameter of the primary spheres making up the agglomerates must be $\leq 0.1 \lambda$. This should be viewed as a general guideline; the actual size limit will depend on the optical properties of the particle. The typical primary size of soot is in the range 30–50 nm, which is within or, at least, close to be the limit for visible wavelengths. Second, the fractal dimension must be less than 2, so that there is a minimal amount of multiple scattering. A dimensionality less than 2, which is the case for smoke agglomerates, means that most of the primary spheres making up the agglomerate are visible on a projected image with few totally blocked by spheres above or below.

The validity of the Rayleigh–Debye method is still of concern. There have been several theoretical studies to assess the effect of multiple scattering. These analyses treat multiple scattering as a coupling between the dipole fields from the primary spheres. The electric field arising from *n*th dipole (primary sphere) affects the electric field at every other sphere and, vice versa, the field arising

[®] Abstract published in *Advance ACS Abstracts*, July 1, 1994.

(1) Schaefer, D. W.; Martin, J. E.; Wiltzius, P.; Cannell, D. S. *Phys. Rev. Lett.* **1984**, *52*, 2371.

(2) Martin, J. E.; Schaefer, D. W.; Hurd, A. J. *J. Phys. Rev. A* **1986**, *33*, 3540.

(3) Mountain, R. D.; Mulholland, G. W. *Langmuir* **1988**, *4*, 1321.

(4) Sorensen, C. M.; Cai, J.; Lu, N. *Appl. Opt.* **1992**, *31*, 6547.

(5) Hall, R. J.; Bonczyk, P. A. *Langmuir* **1991**, *7*, 1274.

(6) Berry, M. V.; Percival, I. C. *Opt. Acta* **1986**, *33*, 577.

(7) Colbeck, I.; Hardman, E. J.; Harrison, R. M. *J. Aerosol Sci.* **1989**, *20*, 765.

from every other dipole (primary sphere) contributes to the field at the n th sphere. This coupled dipole analysis was shown by Lakhtakia *et al.*⁸ to be equivalent to a discretized version of an integral formulation of the Maxwell curl equations. Nelson⁹ used this method to calculate total scattering and absorption cross sections of agglomerates up to size 50 spheres. She obtained agreement within 10% with Rayleigh–Debye scattering predictions. Iskander *et al.*¹⁰ used the method of moments to compute the absorption cross section of agglomerates with up to 256 spheres. They report up to 50% enhanced absorption relative to the Rayleigh–Debye prediction for certain primary particle sizes. Singham and Bohren¹¹ computed differential cross sections for agglomerates with fractal dimension of about 1.8 and 2.5 and with up to 10^3 primary spheres for primary sphere diameter of 0.1λ . They report small differences relative to the Rayleigh–Debye for both the intensity and degree of linear polarization for incident unpolarized light. They were able to solve for the coupled dipole fields for these large clusters by using the scattering order method,¹² which is based on successive approximations. The same general solution method is used in this study.

Although the coupled dipole method allows treatment of multiple scattering, it is still limited to a primary sphere size parameter x , defined as the ratio of the particle circumference to wavelength, less than about 0.5. For larger x , scattering by an individual sphere is poorly represented by treating each primary sphere as a point dipole. One approach to treating the finite size of the primary sphere is to subdivide each sphere into several dipoles. This approach was used by Kattawar and Humphreys¹³ and Flatau *et al.*¹⁴ for two spheres. West¹⁵ used this approach to compute the optical properties of a 170 unit agglomerate grown by diffusion-limited aggregation with each primary unit subdivided into 22 dipoles; he also treated 8 primary units, each subdivided into 421 dipoles. A limitation of multiple dipoles to approximate a primary particle is the large number of dipole elements required for the calculation.

In this paper we take a different tack by extending the coupled dipole method to larger x by including both the electric and magnetic dipole moments. We term this method the coupled electric and magnetic dipole method (CEMD) and abbreviate the coupled electric dipole method as CED. The approach is a straightforward generalization of the CED method. The method is analogous to the theoretical development by Singham¹⁶ to treat the intrinsic optical activity of a particle of arbitrary shape. Coupled equations are obtained for both exciting electric and magnetic fields. For the method to be useful it must at least provide accurate results for a single sphere. As shown in section II, including the magnetic dipole term results in accurate differential and total cross sections for size parameter ≤ 1 for a single sphere. The basic equations for coupled electric and magnetic dipoles are formulated and the solution method is described in section III. The

results for the differential and total scattering cross sections are given in section IV. Expressions for small-angle scattering are also derived in the limit of no dipole coupling. In section V results for two spheres are compared with exact results obtained by using the order-of-scattering-method described by Fuller.¹⁷ In section VI results are presented for clusters grown by Brownian dynamics with 17, 52, and 165 primary spheres. Results are presented for particles with refractive index similar to that of soot ($n = 1.7 + 0.7i$) and similar to that of silica ($n = 1.55$). The following commonly measured quantities are calculated: total scattering and absorption cross sections, differential scattering for vertically polarized incident light, and the polarization ratio. The small angle results are analyzed to assess the effects of multiple scattering and the primary sphere size on the inferred radius of gyration and scattering intensity at $\theta = 0$. Polarization results are shown to be sensitive to the primary sphere size.

II. Comparison of the Electric Dipole, the Electric and Magnetic Dipole, and Lorenz–Mie Results for a Single Sphere

The focus of this paper is the development of a method for computing light scattering by agglomerates with size parameter x for the primary sphere up to about 1. This corresponds to a primary sphere diameter of about $0.2\ \mu\text{m}$ for scattering at the He–Ne laser wavelength. The basic approach is to include the first two terms in the multipole expansion for scattering by a sphere: the electric and the magnetic dipole terms. In the next section we extend the coupled dipole method to include the magnetic dipole term. As a preamble to this analysis, we compare the cross sections computed for a single sphere based on the first term in the Lorenz–Mie (LM) expansion, the electric dipole term, on the first two terms, the electric and magnetic dipole terms, and on all multipoles. One expects that improving the computed cross section of a single primary sphere will lead to improved cross section for the agglomerate.

The extinction cross section, σ_e , and the total scattering cross section, σ_s , are obtained as sums over the LM coefficients

$$\sigma_s = \frac{2\pi}{k^2} \sum_n (2n+1)(|a_n|^2 + |b_n|^2) \quad (1)$$

$$\sigma_e = \frac{2\pi}{k^2} \sum_n (2n+1) \text{Re}(a_n + b_n) \quad (2)$$

The cross sections for the electric dipole term (σ_e^E and σ_s^E), correspond to the a_1 term

$$\sigma_s^E = \frac{6\pi}{k^2} |a_1|^2 \quad (3)$$

$$\sigma_e^E = \frac{6\pi}{k^2} \text{Re}(a_1) \quad (4)$$

The analogous expressions for an electric and a magnetic dipole are given by

$$\sigma_s^{\text{EM}} = \frac{6\pi}{k^2} (|a_1|^2 + |b_1|^2) \quad (5)$$

(8) Lakhtakia, A.; Mulholland, G. W. *J. Res. Natl. Inst. Stand. Technol.*, in press.

(9) Nelson, J. *J. Mod. Opt.* **1989**, *36*, 1031.

(10) Iskander, M. F.; Chen, H. Y.; Penner, J. E. *Atmos. Environ.* **1991**, *25A*, 2563.

(11) Singham, S. B.; Bohren, C. F. *Langmuir* **1993**, *9*, 1431.

(12) Singham, S. B.; Bohren, C. F. *J. Opt. Soc. Am. A: Opt. Image Sci.* **1988**, *5*, 1867.

(13) Kattawar, G. W.; Humphreys, T. J. *Light Scattering by Spherical Particles*; Schuerman, D. W., Ed.; Plenum Press: New York, 1980; p 177.

(14) Flatau, P. J.; Fuller, K. A.; Mackowski, D. W. *Appl. Opt.*, in press.

(15) West, R. A. *Appl. Opt.* **1991**, *30*, 5316.

(16) Singham, S. B. *Chem. Phys. Lett.* **1986**, *130*, 139.

(17) Fuller, K. A. *Appl. Opt.* **1991**, *30*, 4716.

$$\sigma_e^{\text{EM}} = \frac{6\pi}{k^2} \text{Re}(a_1 + b_1) \quad (6)$$

An approximation for σ_s^{E} widely used in the combustion community is to approximate a_1 by the first term in the expansion of a_1 for small x ^{18,19}

$$a_1 \approx -\frac{i2x^3 m^2 - 1}{3 m^2 + 2} \quad (7)$$

where m is the refractive index of the particle relative to the surrounding medium. The symbol σ_s^{R} is used to represent this so-called Rayleigh approximation. The ratio of σ_s^{E} , σ_s^{EM} , and σ_s^{R} to the value for σ_s for the LM expansion is plotted in Figure 1 for a refractive index of $1.7 + 0.7i$, which is similar to that of soot agglomerates. The quantity σ_s^{R} deviates by about 5% from the LM result at $x \approx 0.7$, at $x \approx 1$ for σ_s^{E} , and at $x \approx 1.4$ for σ_s^{EM} . For a refractive index similar to that of silica, $m = 1.55$, the deviations are slightly less compared with those for the sootlike sphere. The inclusion of the magnetic dipole has a greater impact on the absorption cross section. As indicated in Figure 2 the inclusion of the magnetic dipole doubles the range of 5% accuracy to $x = 0.8$ compared to $x = 0.4$ for the dielectric dipole. The absorption cross section is computed from the difference between the extinction cross section and the scattering cross section. One expects that including the magnetic dipole term would also lead to more accurate cross sections for agglomerates.

The angular scattering pattern is characterized by the differential scattering cross sections, $\sigma_h(\theta)$ and $\sigma_v(\theta)$, for incident light polarized horizontally and vertically, respectively, to the scattering plane. The expressions for the differential scattering cross sections are

electric dipole (ED)

$$\sigma_v^{\text{E}}(\theta) = \frac{9}{4k^2} |a_1|^2 \quad (8)$$

$$\sigma_h^{\text{E}}(\theta) = \frac{9}{4k^2} |a_1|^2 \cos^2 \theta \quad (9)$$

electric and magnetic dipole result (EMD)

$$\sigma_v^{\text{EM}}(\theta) = \frac{9}{4k^2} [|a_1|^2 + |b_1|^2 \cos^2 \theta + \cos \theta (a_1 b_1^* + a_1^* b_1)] \quad (10)$$

$$\sigma_h^{\text{EM}}(\theta) = \frac{9}{4k^2} [|b_1|^2 + |a_1|^2 \cos^2 \theta + \cos \theta (a_1 b_1^* + a_1^* b_1)] \quad (11)$$

Scattering by an electric dipole is independent of angle for the v polarization while scattering by a magnetic dipole is independent of angle for the h polarization. The effect of the magnetic dipole is to enhance the forward scattering versus backscattering for vertically polarized light. This result is true provided m is not too large; for small metallic

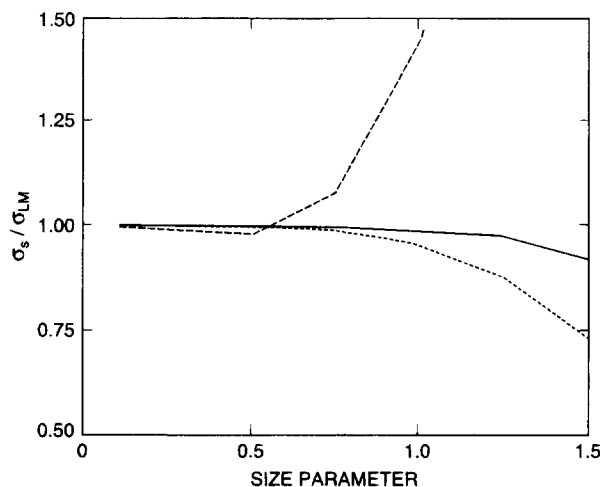


Figure 1. Ratio of the total scattering cross section to the Lorenz-Mie (LM) result versus primary sphere size parameter x for $m = 1.7 + 0.7i$ (σ_s^{EM} solid line, σ_s^{E} short dash, and σ_s^{R} long dash).

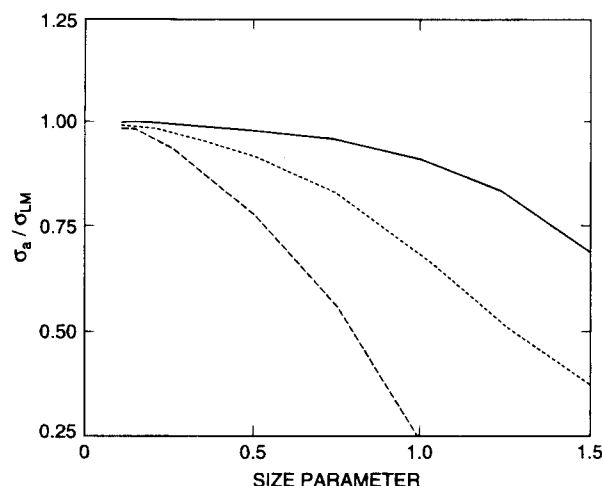


Figure 2. Ratio of absorption cross section to the LM result versus primary sphere size parameter x for $m = 1.7 + 0.7i$ (σ_a^{EM} solid line, σ_a^{E} short dash, and σ_a^{R} long dash).

particles eqs 10 and 11 do not apply and backscattering is greater than forward scattering as is discussed by van de Hulst.¹⁸

The polarization ratio, σ_h/σ_v , is commonly measured, and, as will be apparent below, may be an indicator of primary particle size even for an agglomerate. For $\theta = 90^\circ$, the following result is obtained in the limit of small x for a real refractive index:

$$\frac{\sigma_h^{\text{EM}}(90^\circ)}{\sigma_v^{\text{EM}}(90^\circ)} = \left(\frac{x^2(m^2 + 2)}{30} \right)^2 \quad (12)$$

This ratio would be zero for electric dipole scattering. Terms to order x^5 are included in the expansion of the LM coefficients a_1 and b_1 .

As seen in Figures 3 and 4 for $x = 1$, $\lambda = 0.6328$, and $m = 1.7 + 0.7i$, the inclusion of the magnetic dipole term qualitatively captures the enhanced forward scattering and the finite polarization ratio predicted by LM theory. Without the magnetic dipole term, the shape of the differential scattering plots is qualitatively different from the LM results. For the silica-like particle with $m = 1.55$, the EMD polarization ratio is in poorer agreement with LM theory than for the sootlike particle with $m = 1.7 + 0.7i$.

(18) van de Hulst, H. C. *Light Scattering by Small Particles*; Wiley: New York, 1957.

(19) Bohren, C. F.; Huffman, D. R. *Absorption and Scattering of Light by Small Particles*; Wiley-Interscience: New York, 1983.

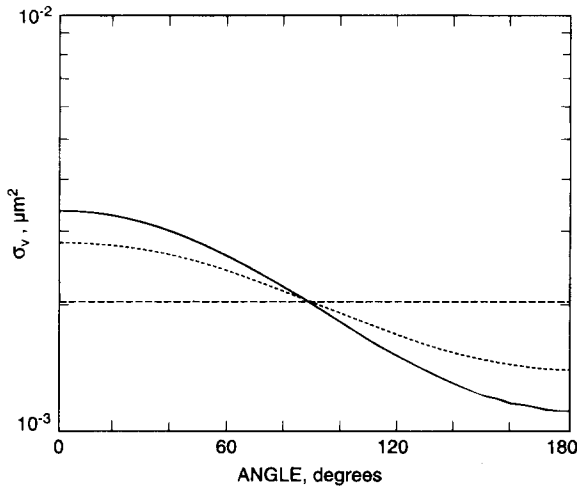


Figure 3. Differential scattering cross section for vertically polarized light plotted versus angle for $x = 1$ and $m = 1.7 + 0.7i$ (LM result solid line, σ_v^{EM} short dash, σ_v^{E} long dash).

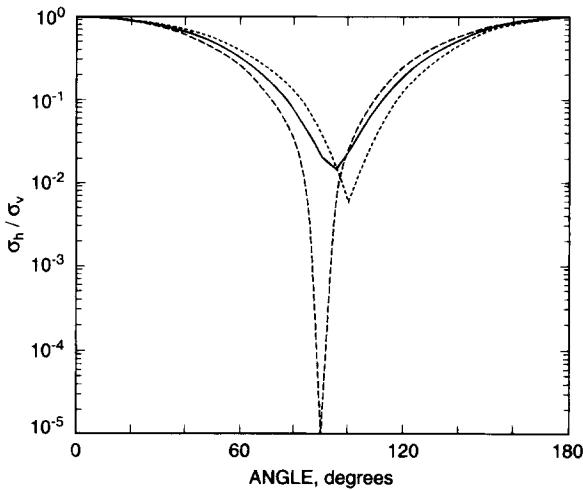


Figure 4. Polarization ratio plotted versus angle for $x = 1$ and $m = 1.7 + 0.7i$ (LM result solid line, $\sigma_h^{\text{EM}}(\theta)/\sigma_v^{\text{EM}}(\theta)$ short dash, $\sigma_h^{\text{E}}(\theta)/\sigma_v^{\text{E}}(\theta)$ long dash).

So we see that including the magnetic dipole increases the size parameter x to about 1 for accurate total cross section results and provides at least qualitative agreement with LM results for differential scattering for $x = 1$. Further improvement in the agreement could be obtained by including the contribution of the LM coefficient a_2 , the quadrupole term, since it has a leading order x^5 dependence, the same as the magnetic dipole term. While the addition is straightforward for the single sphere and is generally included in the first-order correction to Rayleigh scattering,¹⁸ it is not done here because of the added complexity of treating a large agglomerate with interacting quadrupole moments in addition to electric and magnetic dipole moments.

III. Coupled Electric and Magnetic Dipole Equation

The analysis presented below is an adaptation of Singham's treatment of coupled electric and magnetic dipoles¹⁶ to a smoke agglomerate, where each primary unit is treated as a dipole. The fields \vec{E}_p and \vec{H}_p ²⁰ from an electric dipole, \vec{p} , a distance r and direction \vec{n} from the dipole can be expressed in the following form in SI units:

$$\vec{E}_p = \frac{1}{4\pi\epsilon_0} \left[\vec{p} \frac{e^{ikr}}{r} \left(k^2 - \frac{1}{r^2} + \frac{ik}{r} \right) + \vec{n}(\vec{n} \cdot \vec{p}) \frac{e^{ikr}}{r} \left(-k^2 + \frac{3}{r^2} - \frac{3ik}{r} \right) \right] \quad (13)$$

$$\vec{H}_p = \frac{1}{4\pi(\mu_0\epsilon_0)^{1/2}} \left[(\vec{n} \times \vec{p}) \frac{e^{ikr}}{r} \left(k^2 + \frac{ik}{r} \right) \right] \quad (14)$$

The corresponding expressions for the fields \vec{E}_m and \vec{H}_m ²⁰ from a magnetic dipole, \vec{m} , are given by

$$\vec{E}_m = -\frac{1}{4\pi(\epsilon_0)^{1/2}} (\vec{n} \times \vec{m}) \frac{e^{ikr}}{r} \left(k^2 + \frac{ik}{r} \right) \quad (15)$$

$$\vec{H}_m = \frac{1}{4\pi} \left[\vec{m} \frac{e^{ikr}}{r} \left(k^2 - \frac{1}{r^2} + \frac{ik}{r} \right) + \vec{n}(\vec{n} \cdot \vec{m}) \frac{e^{ikr}}{r} \left(-k^2 + \frac{3}{r^2} - \frac{3ik}{r} \right) \right] \quad (16)$$

The electric and magnetic dipole moments for a sphere for incident plane wave fields \vec{E}_0 and \vec{H}_0 are given by

$$\vec{p} = \epsilon_0 \alpha_E \vec{E}_0 \quad (17)$$

$$\vec{m} = \alpha_H \vec{H}_0 \quad (18)$$

where the electric and magnetic polarizabilities, α_E and α_H , are related to the LM coefficients as follows:

$$\alpha_E = 6\pi a_1/k^3 \quad (19)$$

$$\alpha_H = 6\pi b_1/k^3 \quad (20)$$

In the original formulation of the coupled dipole method by Purcell and Pennypacker,²¹ a_1 was approximated by the first term in the small x expansion. Dungey and Bohren²² used the full expression for a_1 to allow treatment of larger primary units and eq 20 is an extension of their method to the magnetic dipole term.

The electric and magnetic fields at the i th particle resulting from the electric and magnetic dipole moments at the j th particle are obtained from eqs 13–16 with the electric and magnetic dipoles expressed in terms of \vec{E}_j and \vec{H}_j using eqs 17 and 18.

$$\vec{E}_i = a_{ij} \alpha_E \vec{E}_j + b_{ij} \alpha_E (\vec{E}_j \cdot \vec{n}_{ji}) \vec{n}_{ji} - d_{ij} \left(\frac{\mu_0}{\epsilon_0} \right)^{1/2} \alpha_H (\vec{n}_{ji} \times \vec{H}_j) \quad (21)$$

$$\vec{H}_i = a_{ij} \alpha_H \vec{H}_j + b_{ij} \alpha_H (\vec{H}_j \cdot \vec{n}_{ji}) \vec{n}_{ji} + d_{ij} \left(\frac{\epsilon_0}{\mu_0} \right)^{1/2} \alpha_E (\vec{n}_{ji} \times \vec{E}_j) \quad (22)$$

The coefficients a_{ij} , b_{ij} , and d_{ij} are shorthand expressions for the r -dependent functions in eqs 13–16. For example, a_{ij} is given by

$$a_{ij} = \frac{1}{4\pi} \frac{e^{ikr_{ij}}}{r_{ij}} \left(k^2 - \frac{1}{r_{ij}^2} + \frac{ik}{r_{ij}} \right) \quad (23)$$

where r_{ij} is the distance between the i th and j th dipoles.

(21) Purcell, E. M.; Pennypacker, C. R. *Astrophys. J.* **1973**, *186*, 705.

(22) Dungey, C. E.; Bohren, C. F. *J. Opt. Soc. Am. A: Opt. Image Sci.* **1991**, *8*, 81.

(20) Jackson, J. D. *Classical Electrodynamics*, Wiley: New York, 1962.

It is convenient in solving the coupled equations to express the various vector products in eqs 21 and 22 as matrix products.

$$a_{ij}\vec{E}_j + b_{ij}(\vec{E}_j \cdot \vec{n}_{ji})\vec{n}_{ji} = \tilde{C}_{ij}\vec{E}_j \quad (24)$$

where

$$\tilde{C}_{ij} =$$

$$\begin{pmatrix} a_{ij} + b_{ij}(n_{ji}^x)^2 & b_{ij}n_{ji}^x n_{ji}^y & b_{ij}n_{ji}^x n_{ji}^z \\ b_{ij}n_{ji}^y n_{ji}^x & a_{ij} + b_{ij}(n_{ji}^y)^2 & b_{ij}n_{ji}^y n_{ji}^z \\ b_{ij}n_{ji}^z n_{ji}^x & b_{ij}n_{ji}^z n_{ji}^y & a_{ij} + b_{ij}(n_{ji}^z)^2 \end{pmatrix} \quad (25)$$

$$d_{ij}(\vec{n}_{ji} \times \vec{H}_j) = \tilde{f}_{ij}\vec{H}_j \quad (26)$$

where

$$\tilde{f}_{ij} = \begin{pmatrix} 0 & -d_{ij}n_{ji}^z & d_{ij}n_{ji}^y \\ d_{ij}n_{ji}^z & 0 & -d_{ij}n_{ji}^x \\ -d_{ij}n_{ji}^y & d_{ij}n_{ji}^x & 0 \end{pmatrix} \quad (27)$$

Also we express the fields in reduced form by normalizing by the magnitude of the incident field.

$$\vec{E}^r = \vec{E}/E_0 \quad (28)$$

$$\vec{H}^r = \vec{H}/H_0 \quad (29)$$

Using eqs 28 and 29, we can express eqs 22 and 23 as

$$\vec{E}_i^r = \alpha_E \tilde{C}_{ij} \vec{E}_j^r + \alpha_H \tilde{f}_{ij} \vec{H}_j^r \quad (30)$$

$$\vec{H}_i^r = \alpha_H \tilde{C}_{ij} \vec{H}_j^r + \alpha_E \tilde{f}_{ij} \vec{E}_j^r \quad (31)$$

The preceding expressions give the fields at the i th particle due to a single dipole. To obtain the total field, we take the sum over all other dipoles. We add to this the contribution from the incident field. This is essentially the same procedure used by Singham.¹⁶

$$\vec{E}_i^r = \vec{E}_i^{r0} + \alpha_E \sum_{j \neq i}^N \tilde{C}_{ij} \vec{E}_j^r + \alpha_H \sum_{j \neq i}^N \tilde{f}_{ij} \vec{H}_j^r \quad (32)$$

$$\vec{H}_i^r = \vec{H}_i^{r0} + \alpha_H \sum_{j \neq i}^N \tilde{C}_{ij} \vec{H}_j^r + \alpha_E \sum_{j \neq i}^N \tilde{f}_{ij} \vec{E}_j^r \quad (33)$$

To solve these equations, we use successive approximations. In eqs 32 and 33 we substitute the incident plane wave fields, \vec{E}_j^{r0} and \vec{H}_j^{r0} , for \vec{E}_j^r and \vec{H}_j^r and compute a first-order estimate, \vec{E}_i^{r1} and \vec{H}_i^{r1} for every particle. Then the entire procedure is repeated with the first-order estimates of the fields, \vec{E}_j^{r1} and \vec{H}_j^{r1} , substituted in eqs 32 and 33 for \vec{E}_j^r and \vec{H}_j^r . This procedure is repeated until successive approximations agree to within a desired amount.

The exciting fields for two spheres in contact are given in Table 1. In the Rayleigh–Debye approximation the exciting fields is just the incident field. We refer to the difference between the exciting field and the incident field as the coupling field. The exciting field is computed for end-on incidence, where the axis of the centers of the two spheres is aligned parallel to the direction of light propagation, and for broadside incidence, where the axis is perpendicular to the direction of propagation and is

Table 1. Successive Approximations for Exciting Fields for Two Spheres in Contact (Parameters: $m = 1.7 + 0.7i$, $\lambda = 0.6328 \mu\text{m}$)

sphere no.	incident field		ex field, 1st iteration		ex field, 5th iteration ^a	
	Re	Im	Re	Im	Re	Im
$\pi D/\lambda = 0.1$, End-On Incidence ^b						
1	1.000	0.000	0.961	-0.051	0.963	-0.048
2	0.921	0.389	0.864	0.358	0.865	0.362
$\pi D/\lambda = 0.1$, Broadside Parallel ^c						
1	1.000	0.000	1.125	0.081	1.134	0.105
2	1.000	0.000	1.125	0.081	1.134	0.105
$\pi D/\lambda = 1.0$, End-On Incidence						
1	1.000	0.000	0.936	0.112	0.905	0.076
2	-0.654	-0.757	-0.316	-0.909	-0.299	-0.898
$\pi D/\lambda = 1.0$, Broadside Parallel						
1	1.000	0.000	0.926	-0.077	0.926	-0.066
2	1.000	0.000	0.926	-0.077	0.926	-0.066

^a For the examples given in this table, the fifth iteration agrees with higher order iterations to within ± 0.001 . ^b End on incidence corresponds to the axis defined by the centers of the two spheres being parallel to the direction of light propagation. Particle 1 is at the origin of the coordinate system. ^c Broadside parallel corresponds to the doublet axis being perpendicular to the direction of light propagation and parallel to the the light polarization direction.

parallel to the direction of the laser polarization. Even for the small particle diameter D with $\pi D/\lambda = 0.1$, the contribution of the coupling field is about 12% of the incident field for the broadside orientation. The fact that the coupling field does not vanish for small particle size has important implications for the validity of the Rayleigh–Debye approximation as discussed in the last section. The far-field results including the total and differential scattering cross sections are presented in section V for this case of two spheres in contact.

Our convergence criterion is that the total forward scattered intensity differs by less than 0.1% for two successive approximations. For $x \leq 0.25$, typically 5–6 iterations were required for agglomerates with up to 165 primary spheres for a fractal dimension of about 1.9 and about 10 iterations were required for $x = 0.5$. For $x = 1$, convergence was obtained after about 12 iterations for 52 spheres and was not obtained for the agglomerate with 165 spheres. The failure of the iteration method to converge is a result of the increasing effect of the coupling fields with increasing x , as indicated in Table 1, and the increasing number of dipole–dipole interactions with increasing agglomerate size.

The successive approximation method failed to give a solution for two overlapping spheres. The dipole field at the second sphere induced by the first sphere may be larger than the incident field. For example, if the distance between the center of the particles is a particle radius, a , instead of $2a$, the value of r in eq 13 would be reduced by a factor of 2 so that the $1/r^3$ term in eq 13 would be increased by a factor of 8. Significant overlap between the spheres occurred in some of the simulations of particle agglomeration. Another situation where the successive approximation method may not yield a solution for the same reason as above is for a large and small sphere in contact. In these cases another solution method such as the conjugate gradient method must be applied to the set of equations defined by eqs 32 and 33.

IV. Far-Field Solution

In order to compute the cross sections, one must obtain the far-field scattering solution. The far fields for an

electric and magnetic dipole correspond to the $1/r$ terms in eqs 13 and 15, respectively. The electric and magnetic dipole for the i th primary particle is computed from eqs 17 and 18 with the exciting fields \vec{E}_i and \vec{H}_i substituting for \vec{E}_0 and \vec{H}_0 . The contribution from all the dipoles is obtained as a sum over i . The final result can be expressed in terms of \vec{n}_d , the unit vector directed toward the detector, and r_d , the distance from the origin of the agglomerate coordinate system to the detector.

$$\vec{E}_d^r = \frac{k^2 e^{ikr_d}}{4\pi r_d} [\alpha_E (\vec{I} - \vec{n}_d \vec{n}_d) (\sum_{i=1}^N e^{-ik\vec{r}_i \cdot \vec{n}_d} \vec{E}_i^r) - \alpha_H \vec{n}_d \times (\sum_{i=1}^N e^{-ik\vec{r}_i \cdot \vec{n}_d} \vec{H}_i^r)] \quad (34)$$

The following approximations based on r_d much larger than r_i are made in obtaining eq 34

$$\vec{n}_{id} = \frac{\vec{r}_d - \vec{r}_i}{r_{id}} \approx \vec{n}_d = \frac{\vec{r}_d}{r_d} \quad (35)$$

$$r_{id} = r_d - \vec{r}_i \cdot \vec{n}_d \quad (36)$$

The scattering properties are conveniently expressed in terms of the scattering amplitude vectors \vec{X} and \vec{Y} and the scattering amplitude coefficients.¹⁹ For x -polarized incident light, \vec{X} is related to \vec{E}_d^r by the following equation:

$$\vec{E}_d^r = \frac{e^{ikr_d}}{-ikr_d} \vec{X} \quad (37)$$

A similar expression is obtained for the y -polarized light. The total scattering cross section, σ_s , for x -polarized light¹⁹ is obtained as

$$\sigma_s = \int_0^{2\pi} \int_0^\pi \frac{|\vec{X}|^2}{k^2} \sin \theta \, d\theta \, d\phi \quad (38)$$

Henceforth, instead of denoting orthogonal directions by x and y , we shall use v and h , where v indicates vertical and h horizontal. Moreover, the v direction is perpendicular to the scattering plane and the h direction is parallel to this plane. Scattering cross sections depend on the state of polarization of the incident light and on any analyzer placed forward to the detector. This dependence is indicated by appending two subscripts to cross sections: the first indicates the state of linear polarization of the incident light and the second indicates the orientation of the linear analyzer. For example, $\sigma_{vv}(\theta)$, is the cross section for incident vertically polarized light measured by a detector preceded by an analyzer that passes light of this polarization. The differential scattering cross sections are conveniently expressed in terms of the scattering amplitude coefficients, which are defined via the matrix relationship between the plane incident fields and the scattered fields:

$$\begin{pmatrix} \vec{E}_{hs} \\ \vec{E}_{vs} \end{pmatrix} = \frac{e^{ik(r-z)}}{-ikr} \begin{pmatrix} S_2 & S_3 \\ S_4 & S_1 \end{pmatrix} \begin{pmatrix} \vec{E}_{hi} \\ \vec{E}_{vi} \end{pmatrix} \quad (39)$$

The differential cross sections are related to the scattering amplitudes as follows:¹⁹

$$\sigma_{vv}(\theta) = \frac{|S_1|^2}{k^2}, \quad \sigma_{hh}(\theta) = \frac{|S_2|^2}{k^2}, \quad \sigma_{vh}(\theta) = \frac{|S_3|^2}{k^2}, \quad \sigma_{hv}(\theta) = \frac{|S_4|^2}{k^2} \quad (40)$$

The sum of all these components is equal to the scattering of unpolarized light, $\sigma(\theta)$.

$$\sigma(\theta) = \frac{1}{k^2} [|S_1|^2 + |S_2|^2 + |S_3|^2 + |S_4|^2] \quad (41)$$

This quantity $\sigma(\theta)$ is used as an indicator of the convergence of the successive approximation calculations. From eqs 37 and 39, we obtain the following expressions for the scattering amplitude coefficients:

$$S_1 = \vec{e}_{vs} \cdot \vec{Y}, \quad S_2 = \vec{e}_{hs} \cdot \vec{X}, \quad S_3 = \vec{e}_{hs} \cdot \vec{Y}, \quad S_4 = \vec{e}_{vs} \cdot \vec{X} \quad (42)$$

The unit vectors \vec{e}_{hs} and \vec{e}_{vs} are related to the x , y , and z unit vectors in the following way for $\phi = 0$:

$$\vec{e}_{hs} = \cos \theta \vec{e}_x - \sin \theta \vec{e}_z \quad (43)$$

$$\vec{e}_{vs} = -\vec{e}_y \quad (44)$$

The expressions for S_1 and S_2 will be needed below for analysis of small-angle scattering and determination of the extinction cross section. They are obtained from eqs 42, 43, and 44 and the expressions for \vec{X} and \vec{Y}

$$S_1 = \frac{ik^3}{4\pi} [\alpha_E S_{yy} - \alpha_H (\cos \theta S_{Hyx} - \sin \theta S_{Hyx})] \quad (45)$$

$$S_2 = \frac{-ik^3}{4\pi} [\alpha_E (S_{xx} \cos \theta - S_{xz} \sin \theta) + \alpha_H S_{Hxy}] \quad (46)$$

The first subscript in the sum S_{yy} refers to the direction of polarization of the incident light and the second to the x , y , or z vector component. For example,

$$S_{yy} = \sum_{i=1}^N e^{-ik\vec{r}_i \cdot \vec{n}_d} \vec{E}_i^{ryy} \quad (47)$$

$$S_{Hyx} = \sum_{i=1}^N e^{-ik\vec{r}_i \cdot \vec{n}_d} H_i^{ryx} \quad (48)$$

The extinction cross section is computed using the extinction theorem, which for x polarized light can be expressed as¹⁹

$$\sigma_e^x = \frac{4\pi}{k^2} \text{Re}[(\vec{X} \cdot \vec{e}_x)_{\theta=0}] \quad (49)$$

From the second part of eq 42 we see that $\vec{X} \cdot \vec{e}_x$ evaluated at $\theta = 0$ is just $S_2(\theta=0)$. Substituting the expression for S_2 into eq 46 and simplifying, we obtain

$$\sigma_e^x = k \text{Im} (\alpha_E \sum_{i=1}^N e^{-ikz_i} \vec{E}_i^{rxx} + \alpha_H \sum_{i=1}^N e^{-ikz_i} H_i^{rxy}) \quad (50)$$

We see that the differential and the total cross sections can be computed from a knowledge of the exciting local fields, the relative location of the primary spheres, and the properties of the spheres.

The extinction theorem does not give a useful result for the RD method applied to an agglomerate. The extinction

theorem expresses extinction as an interference between the incident and forward scattered waves. If both waves have the same phase, the interference is zero and there is no extinction. This is basically the case for the RD approximation. For real refractive index, to first order α is real and the extinction is zero. Even if the next order term is included for α , which is complex, the extinction cross section is proportion to N rather than N^2 . Instead of using the extinction theorem, we compute the extinction cross section for the RD method by adding the scattering cross section to N times the absorption cross section of a single sphere. Before comparing the results of the RD and coupled dipole methods with the exact solution for two spheres, we consider the small-angle behavior of the scattering function.

Small-Angle Scattering. It is of interest to compute the vv scattered intensity at small angles, since small-angle scattering measurements are used to determine the radius of gyration of an agglomerate.^{2,4,5} In our calculations, we compute scattering by a particle in one orientation, while measurements for suspensions of particle agglomerates are necessarily orientation averages unless efforts are made to orient the agglomerates. The explicit expression for S_1 is given by

$$S_1 = \frac{ik^3}{4\pi} [\alpha_E \sum_{i=0}^N e^{-ik\vec{r}_i \cdot \vec{n}_d} E_i^{ryy} - \alpha_H (\cos \theta \sum_{i=1}^N e^{-ik\vec{r}_i \cdot \vec{n}_d} H_i^{ryx} - \sin \theta \sum_{i=1}^N e^{-ik\vec{r}_i \cdot \vec{n}_d} H_i^{ryz})] \quad (51)$$

A first-order estimate of S_1 is obtained by approximating the local exciting fields \vec{E}_i^r and \vec{H}_i^r by the incident plane wave fields. This is a generalized Rayleigh-Debye approximation including the magnetic dipole term. The standard Rayleigh-Debye approximation corresponds to $\alpha_H = 0$. For a y -polarized incident field, we have

$$E_i^{ryy} = e^{ikz}, \quad H_i^{ryx} = -e^{ikz}, \quad H_i^{ryz} = 0 \quad (52)$$

Substituting from eq 52 into eq 51 and expressing the result in terms of the momentum transfer vector \vec{q} , we obtain

$$S_1 = \frac{ik^3}{4\pi} [(\alpha_E + \alpha_H \cos \theta) \sum_{i=1}^N e^{-i\vec{q} \cdot \vec{r}_i}] \quad (53)$$

where

$$\vec{q} = k(\vec{n}_d - \vec{e}_z); \quad |\vec{q}| = \frac{4\pi}{\lambda} \sin\left(\frac{\theta}{2}\right) \quad (54)$$

In the limit of $|\vec{q} \cdot \vec{r}_i| \ll 1$, we expand the exponential and obtain to order q^2

$$S_1 = \frac{ik^3 N}{4\pi} [(\alpha_E + \alpha_H \cos \theta)(1 - iqR_{cm}^q - 1/2q^2(R_g^q)^2)] \quad (55)$$

where R_{cm}^q refers to the q -component of the center of mass of the agglomerate and R_g^q refers to the q -component of the second moment of the mass distribution:

$$R_{cm}^q = \frac{1}{N} \sum_{i=1}^N r_i^q; \quad (R_g^q)^2 = \frac{1}{N} \sum_{i=1}^N (r_i^q)^2 \quad (56)$$

The quantity R_g^q is analogous to the more familiar radius of gyration that appears in the q expansion for orientation

averaged scattering. The small q expansion for $\sigma_{vv}(q)$ is obtained from eqs 39, 55, and the small q expansion of $\cos \theta$. It is convenient to express the result normalized by the scattering at $q = 0$.

$$\frac{\sigma_{vv}(q)}{\sigma_{vv}(q=0)} = 1 - q^2 \left[(R_g^{1q})^2 + \frac{\lambda}{2\pi} \frac{(|\alpha_H|^2 + 1/2 \alpha_H \alpha_E^* + 1/2 \alpha_H^* \alpha_E)}{|\alpha_E + \alpha_H|^2} \right] \quad (57)$$

where the 1 in the superscript expression for R_g^{1q} indicates that R_g^q is computed in a coordinate system at the center of mass of the agglomerate.

In the limit $\alpha_H = 0$ we obtain the standard small q result³ except for the factor of 1/3, which is missing because we are not performing an orientational average. The second term in the brackets will be most significant for large primary sphere size. Even for large primary spheres, the second term will be small relative to the first term for large agglomerates, since the first term increases approximately linearly with N while the second is constant.

Of course the most realistic case is that of interacting dipoles. In section VI we compare R_g^{1q} computed from the small q scattering for the coupled dipole calculation with the actual value based on the coordinates of the primary spheres in the agglomerate.

V. Comparison with Exact Two Sphere Solution

One test of the accuracy of the coupled electric and magnetic dipole method (CEMD) is to compare with the exact solution for two spheres. The first comprehensive, computationally viable solutions to the two-sphere problem were obtained by Liang and Lo²³ and Bruning and Lo²⁴ as a self-consistent set of linear equations for the scattering coefficients. Building on the work of Lo and his colleagues, Fuller and Kattawar developed an order-of-scattering (OS) solution for the problem of scattering and absorption of electromagnetic radiation by linear chains²⁵ and arbitrarily configured clusters²⁶ of spheres. Calculations based on this latter method are often more efficient than those based on the method of Bruning and Lo and may briefly be described as follows: (1) An incident, not necessarily planar, radiation field couples to the normal modes, or multipoles, of the primary spheres in an ensemble of spheres. (For plane wave radiation, this coupling is described by Lorenz-Mie theory.) (2) Each of the multipolar components of the radiation scattered by one sphere then couples to every normal mode of all other spheres in the cluster. The coupling can be quantified by solving the resulting boundary value problems. (3) This and subsequent orders of scattered fields are calculated and (4) these partial fields are summed coherently to determine the total scattered field of the cluster. In the case of only two spheres, one can readily develop a multiple scattering solution analogous to that for reflection and transmission by a dielectric slab. The history and treatment of the multiplesphere problem are summarized in a paper by Fuller.¹⁷ For the present study, it was found that mode orders larger than 10 did not contribute significantly to the final result. Also included in the following discussion is the noninteracting spheres approximation (NI), wherein only steps 1 and 4 above are

(23) Liang, C.; Lo, Y. T. *Radio Sci.* **1967**, *2*, 148.

(24) Bruning, J. H.; Lo, Y. T. *IEEE Trans. Antennas Propag.* **1971**, *AP-19*, 378 and 391.

(25) Fuller, K. A.; Kattawar, G. W. *Opt. Lett.* **1988**, *13*, 90.

(26) Fuller, K. A.; Kattawar, G. W. *Opt. Lett.* **1988**, *13*, 1063.

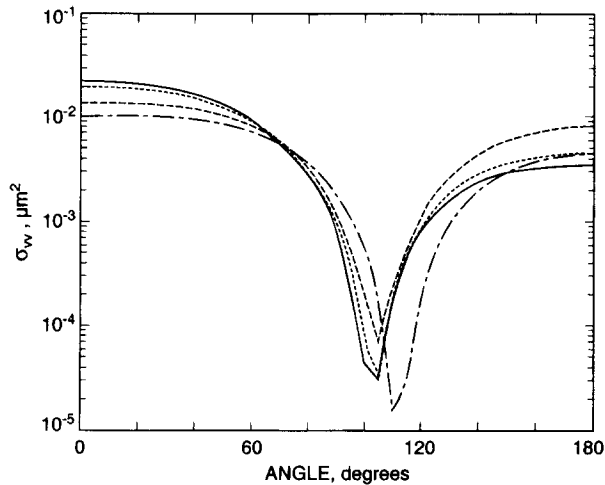


Figure 5. Differential scattering cross section for two spheres for end-on incidence orientation is plotted for vertically polarized light. For the individual spheres $m = 1.8 + 0.5i$, $\lambda = 0.55$, and $x = 1.142$ (OS solid, CEMD short dash, CED long dash, and RD alternating long and short dash).

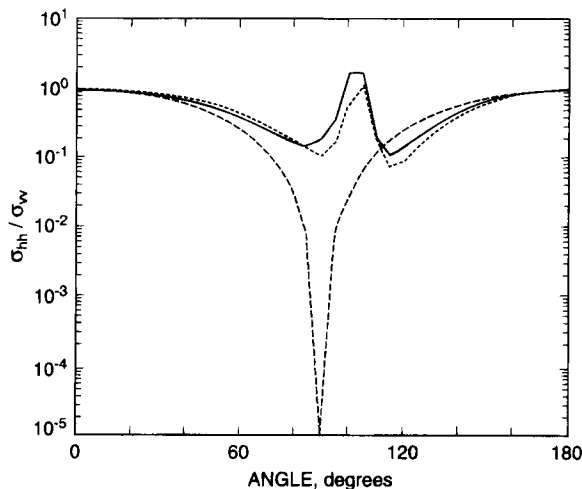


Figure 6. Polarization ratio for two spheres for end-on incidence orientation. For the individual spheres $m = 1.8 + 0.5i$, $\lambda = 0.55$, and $x = 1.142$ (OS solid, CEMD short dash, and CED long dash). The RD results appear identical to the CEO results.

taken. The NI approximation is a generalization of the Rayleigh–Debye method for larger primary sphere size.

Using the OS technique, we computed the differential scattering, total scattering, and absorption cross sections for two spheres in the end-on incidence orientation and in broadside incidence parallel and perpendicular orientations, where parallel and perpendicular refer to the direction of light polarization relative to the axis defined by the centers of the two spheres. The refractive index of the individual spheres is now taken to be $1.8 \pm 0.5i$ with $\lambda = 0.55 \mu\text{m}$. The calculations are carried out for sphere diameters of 0.02, 0.10, and 0.20 μm , which correspond to size parameters of 0.1142, 0.5712, and 1.142. Even for the largest size parameter, we find that the CEMD provides good agreement with the order of scattering result. This is illustrated in Figure 5 for configuration A for vertically polarized light and in Figure 6 for the polarization ratio. The CEMD is in much better agreement with the exact solution than the CED with a 15% underestimate at small angles compared with a 45% underestimate at small angles for CED. The CEMD correctly predicts a peak at about 110° for the polarization ratio while the CED predicts a polarization ratio similar to that of a small sphere with a minimum at 90° . For the

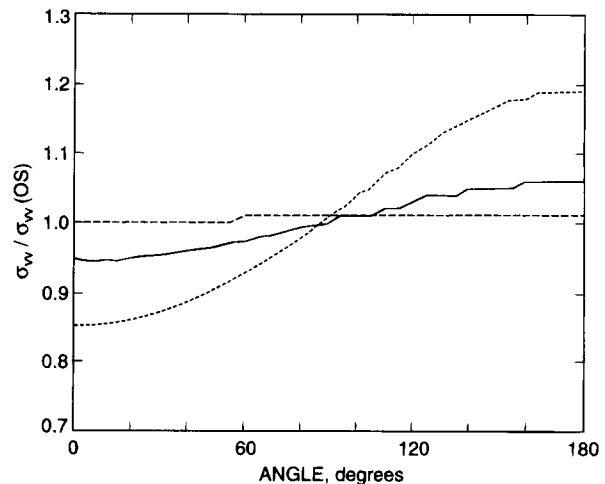
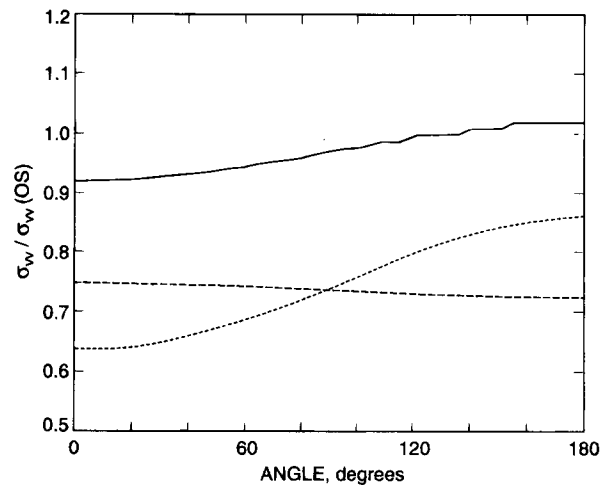


Figure 7. (A, top) The ratio $\sigma_w/\sigma_w(\text{OS})$ is computed for two spheres for broadside parallel orientation with $x = 0.5712$. The distance between the centers of the two spheres is equal to the sphere diameter (spheres are touching) (CEMD solid, RD short dash, and noninteracting multipole long dash). (B, bottom) Same as Figure 7A except the center to center spacing of the spheres is twice the sphere diameter (CEMD solid, RD short dash, and noninteracting multipole long dash).

smaller primary particle sizes the differences between the OS and the CEMD are reduced.

As the spheres are separated, the agreement between CEMD and OS improves slightly; however, there is a large improvement in the agreement between the result of noninteracting multipoles and the OS result. This is illustrated in Figure 7A, where the distance between the centers of the two spheres is equal to the diameter of the sphere (spheres touching), and Figure 7B, where the distance between the centers of the two spheres is twice the diameter of a sphere. It is seen that the noninteracting sphere calculation agrees within a few percent with the OS solution for the separated spheres while the difference is about 25% for the spheres touching. This is an important consideration for large agglomerates, since the average effective spacing will be greater than the nearest neighbor distance and provides hope that the noninteracting calculation may be useful for certain applications.

In Table 2 we compare the results for σ_s and σ_a obtained by the order of scattering and the coupled dipole methods. The CEMD slightly underestimates σ_s by up to 4% while the CED underestimates by up to 14%. There is a larger discrepancy for the absorption cross section. For the largest spheres in the broadside incidence parallel orientation, the CEMD and CED underestimate σ_a by 16% and 50%, respectively. Part of the reason for the under-

Table 2. Comparison of Optical Properties for Two Spheres Computed by Rayleigh–Debye, Coupled Dipole (CEMD and CED), and the Order of Scattering Methods (Parameters: $m = 1.8 + 0.5i$, $\lambda = 0.55 \mu\text{m}$)^a

		Scattering Cross Section			
radius, μm	orientation	$\sigma_s, \mu\text{m}^2$			
		RD	CED	CEMD	OS
0.01	end-on	1.44×10^{-7}	1.29×10^{-7}	1.29×10^{-7}	1.30×10^{-7}
0.01	broadside	1.46×10^{-7}	1.88×10^{-7}	1.88×10^{-7}	1.95×10^{-7}
0.01	broadside \perp	1.46×10^{-7}	1.30×10^{-7}	1.30×10^{-7}	1.31×10^{-7}
0.05	end-on	1.55×10^{-3}	1.37×10^{-3}	1.44×10^{-3}	1.45×10^{-3}
0.05	broadside	2.22×10^{-3}	2.91×10^{-3}	2.91×10^{-3}	3.03×10^{-3}
0.05	broadside \perp	2.08×10^{-3}	1.80×10^{-3}	1.81×10^{-3}	1.81×10^{-3}
0.10	end-on	3.74×10^{-2}	4.94×10^{-2}	5.64×10^{-2}	5.76×10^{-2}
0.10	broadside	6.80×10^{-2}	5.33×10^{-2}	5.69×10^{-2}	5.82×10^{-2}
0.10	broadside \perp	5.27×10^{-2}	3.62×10^{-2}	3.89×10^{-2}	4.01×10^{-2}

		Absorption Cross Section			
radius, μm	orientation	$\sigma_a, \mu\text{m}^2$			
		RD	CED	CEMD	OS
0.01	end-on	5.57×10^{-5}	4.98×10^{-5}	5.00×10^{-5}	5.06×10^{-5}
0.01	broadside	5.57×10^{-5}	7.14×10^{-5}	7.16×10^{-5}	7.60×10^{-5}
0.01	broadside \perp	5.57×10^{-5}	4.96×10^{-5}	4.98×10^{-5}	5.05×10^{-5}
0.05	end-on	8.60×10^{-3}	7.28×10^{-3}	8.20×10^{-3}	8.26×10^{-3}
0.05	broadside	8.60×10^{-3}	1.00×10^{-2}	1.08×10^{-2}	1.18×10^{-2}
0.05	broadside \perp	8.60×10^{-3}	6.61×10^{-3}	7.38×10^{-3}	7.61×10^{-3}
0.10	end-on	8.04×10^{-2}	6.20×10^{-2}	8.31×10^{-2}	8.94×10^{-2}
0.10	broadside	8.04×10^{-2}	3.52×10^{-2}	6.00×10^{-2}	7.18×10^{-2}
0.10	broadside \perp	8.04×10^{-2}	3.09×10^{-2}	5.66×10^{-2}	6.59×10^{-2}

^a Key: RD, Rayleigh–Debye approximation; CED, coupled electric dipole method; CEMD, coupled electric and magnetic dipole method; OS, order of scattering method.

estimate is that the single particle result itself is an underestimate by about 10% for the CEMD and by about 30% for the CED. The effect of primary sphere size on the accuracy of the various methods for computing the absorption cross section for a single sphere was given in Figure 2.

In summary, the CEMD is in quantitative agreement to within 10% with the optical properties of two touching spheres with size parameter of 0.5712 or smaller in terms of total cross section and differential scattering. As the size parameter increases to 1.142, the error increases mainly in the value of σ_a . The results obtained with CEMD are clearly superior to those obtained by CED, just as in the single particle case. Because of the strong coupling effect for two neighboring particles, the Rayleigh–Debye and the noninteracting sphere approximation are in error by as much as 25% even for the smallest spheres. However, as the interparticle spacing increases, these methods provide much better estimates.

VI. Optical Properties of Agglomerates

Generation of Agglomerates. Agglomeration occurs when diffusing primary particles collide and stick together, forming doublets, which in turn collide with primary particles as well as doublets, leading to larger and larger irregularly shaped clusters.²⁷ We begin a simulation of this process by distributing 4000 primary particles of diameter D_p at random positions in a cubic box. There are periodic boundary conditions at the surface of the cube. If there is any overlap between primary particles in the initial distribution, the distribution is discarded and a second distribution of particles is generated. The diffusive motion of a particle of mass m is described by Langevin equations²⁸

$$d\vec{r}/dt = \vec{v}; \quad m d\vec{v}/dt = -m\beta\vec{v} + \vec{f} \quad (58)$$

where \vec{r} and \vec{v} are the position and velocity of the particle, β^{-1} is the momentum relaxation of the agglomerate, and \vec{f} is a random force related to β by the fluctuation–dissipation theorem

$$\langle \vec{f}(t_0) \cdot \vec{f}(t_0 + t) \rangle = 6\beta m k_B T \delta(t) \quad (59)$$

Here k_B is the Boltzmann's constant, T is the absolute temperature of the medium in which the agglomeration process is taking place, and $\delta(t)$ is the Dirac δ function. The diffusive motion of the particles is supplemented by the condition that if any two particles touch, they stick forming a larger, rigid cluster. The cluster continues to diffuse according to the Langevin equation but with a changed mass. This process continues until the desired set of clusters has been generated. This growth process is known in the fractal literature as cluster–cluster aggregation.²⁹

Clusters with up to 700 primary spheres were generated. The agglomerates had a fractal structure over about 1 decade in agglomerate size with a fractal dimension of about 1.9.³ In some of the agglomerates there was a large overlap between two of the primary spheres. The time step in the simulation corresponded to an average movement of only 5% of a particle diameter; however, the relative velocity of two spheres may be greater than the mean leading to a significant overlap in one time step. As discussed in section II, a large overlap between spheres may result in a divergence of the successive approximation method. To minimize the penetration, the interparticle spacing was examined after each collision, and if the interpenetration exceeded 5%, the simulation in effect was reversed for this collision until the pair interpenetrated by less than this 5%. In this study, we have computed the optical properties for three clusters generated in this way with 17, 52, and 165 primary spheres. The XY projections of the agglomerates are illustrated in Figure 8; a listing

(27) Mountain, R. D.; Mulholland, G. W.; Baum, H. J. *Colloid Interface Sci.* **1986**, *114*, 67.

(28) Chandrasekhar, S. *Rev. Mod. Phys.* **1943**, *15*, 1.

(29) Jullien, R.; Botet, *Aggregation and Fractal Aggregates*; World Scientific Publishing: Singapore, 1987.

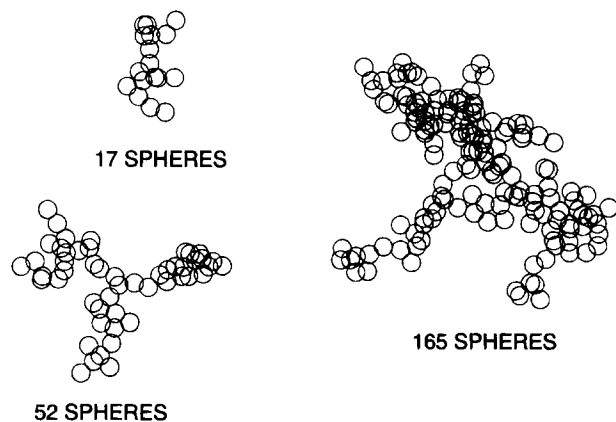


Figure 8. XY-projection of smoke agglomerates of size 17, 52, and 165 primary sphere. The unit of length is the primary particle diameter d_p .

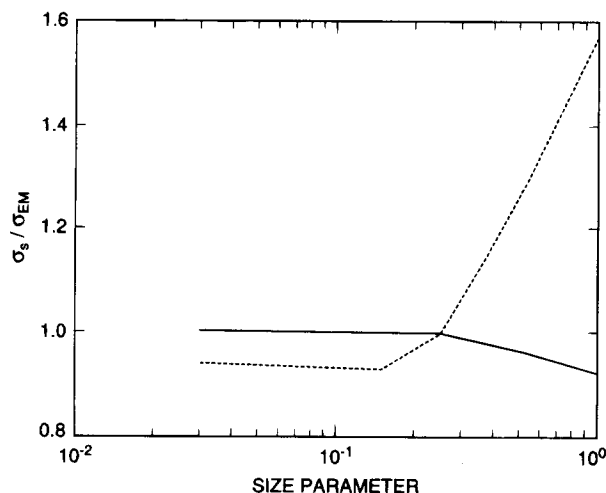


Figure 9. Ratio of the total scattering cross section for CED (solid line) and for RD (dashed line) to the CEMD cross section plotted versus the primary sphere size parameter x for an agglomerate with 52 primary spheres. The refractive index is $1.7 + 0.7i$ and λ is $0.6328 \mu\text{m}$.

of the coordinates can be obtained from the first author. The minimum center-to-center distance for any pair was 0.96 and the average center to center distance for each of the three agglomerates is 0.99.

Total Cross Section for Agglomerates. The extinction cross section σ_e and the total scattering cross section σ_s are computed for the three agglomerates described in the previous section for a refractive indices of $1.7 + 0.7i$ (sootlike) and 1.55 (silica-like). The results are computed for the CEMD, CED, and for RD. The calculations are carried out for a range of primary sphere size parameters from $x = 0.03$ to $x = 1$. As illustrated in Figures 9 and 10, the difference between CEMD and CED for total scattering is less than 2% for $x \leq 0.25$ and then increases to about 10% for $x = 1$ for the sootlike agglomerates and to 20% for the silica-like agglomerates. The RD result is an underestimate for all size parameters for silica while for the soot there is a crossover at $x = 0.25$ from the RD expression being less to greater than the CEMD result. It is as if there is a shielding effect for large primary spheres sizes.

In Figure 11, the absorption cross section divided by N times the absorption cross section of a single sphere is plotted versus x . The single sphere absorption cross section differs for each of the three calculations. Both coupled dipole methods agree within a few percent for $x \leq 0.5$. These results are larger than the RD independent particle approximation for small x and then smaller for

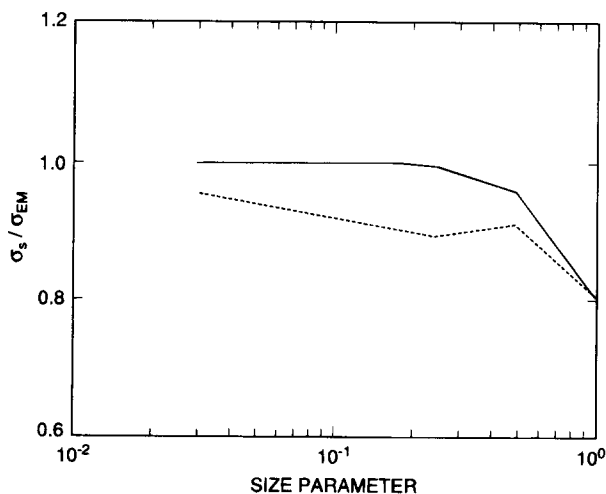


Figure 10. Ratio of the total scattering cross section for CED (solid line) and for RD (dashed line) to the CEMD cross section plotted versus the primary sphere size parameter x for an agglomerate with 52 primary spheres. The refractive index is 1.55 and λ is $0.6328 \mu\text{m}$.

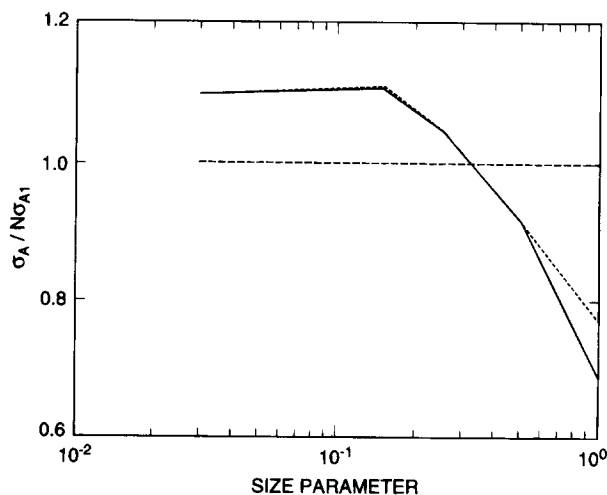


Figure 11. Ratio of the absorption cross section for the 52 sphere agglomerate to N times the single particle value for refractive index equal $1.7 + 0.7i$ versus the primary sphere size parameter x (CEMD solid, CED short dash, and RD long dash).

large x . For small sphere size the exciting field is increased from dipole-dipole coupling resulting in an increase in the absorption cross section, but for large sphere size the dipole-dipole coupling leads to a shielding effect. The CEMD absorption cross section is about 20% greater than the CED cross section for $x = 1$ as indicated in Table 3, where selected results for the scattering and absorption cross sections are presented.

Differential Scattering Plots. Larger differences are obtained in the differential scattering. As indicated in Figure 12 for 17 primary spheres with $x = 0.25$, which is the upper limit of typical smoke size parameter, there is a systematic difference between RD and the coupled dipole calculations of about 20%. The forward scattering difference diminishes as one goes to larger agglomerates as shown in Figure 13 for an agglomerate with 165 primary spheres. For the larger agglomerate there are differences as large as a factor of 10 at angles corresponding to minima but there is still qualitative agreement in the location of the maxima and minima. There is no distinguishable difference between CED and CEMD for $x = 0.25$.

The effect of primary size becomes evident for $x = 1$ as shown in Figures 14 and 15 for the 17 and 52 sphere

Table 3. Comparison of Optical Cross Sections of Selected Agglomerates Computed by the Rayleigh-Debye (RD) and Coupled Dipole (CEMD and CED) Methods ($\lambda = 0.6328 \mu\text{m}$)

Total Scattering Cross Section						
refractive index	no. of primary spheres	size parameter ^a	$\sigma_s, \mu\text{m}^2$			
			RD	CED	CEMD	
1.7 + 0.7i	17	0.25	1.006×10^{-3}	1.062×10^{-3}	1.068×10^{-3}	
	17	0.50	3.377×10^{-2}	2.792×10^{-2}	2.868×10^{-2}	
	17	1.00	5.211×10^{-1}	3.232×10^{-1}	3.510×10^{-1}	
	52	0.25	5.048×10^{-3}	5.056×10^{-3}	5.084×10^{-3}	
	52	0.50	1.051×10^{-1}	8.064×10^{-2}	8.372×10^{-2}	
	52	1.00	1.925	0.9779	1.058	
	165	0.25	2.126×10^{-2}	2.129×10^{-2}	2.157×10^{-2}	
	165	0.50	5.411×10^{-1}	3.546×10^{-1}	3.679×10^{-1}	
	1.55	17	0.25	3.321×10^{-4}	3.603×10^{-4}	3.625×10^{-4}
		17	0.50	1.125×10^{-2}	1.252×10^{-2}	1.298×10^{-2}
17		1.00	2.441×10^{-1}	2.418×10^{-1}	2.787×10^{-1}	
52		0.25	1.666×10^{-3}	1.859×10^{-3}	1.870×10^{-3}	
52		0.50	3.495×10^{-2}	3.688×10^{-2}	3.853×10^{-2}	
52		1.00	7.804×10^{-1}	7.777×10^{-1}	9.714×10^{-1}	
165		0.25	7.019×10^{-3}	7.932×10^{-3}	8.056×10^{-3}	
165		0.50	1.799×10^{-1}	1.961×10^{-1}	2.082×10^{-1}	

Absorption Cross Section					
refractive index	no. of primary spheres	size parameter ^a	$\sigma_a, \mu\text{m}^2$		
			independ-LM ^b	CED	CEMD
1.7 + 0.7i	17	0.03	1.671×10^{-5}	1.799×10^{-5}	1.799×10^{-5}
	17	0.15	2.127×10^{-3}	2.328×10^{-3}	2.342×10^{-3}
	17	0.25	1.015×10^{-2}	1.091×10^{-2}	1.108×10^{-1}
	17	0.50	9.023×10^{-2}	7.472×10^{-2}	7.993×10^{-2}
	17	1.00	7.487×10^{-1}	3.749×10^{-1}	4.806×10^{-1}
	52	0.03	5.110×10^{-5}	5.610×10^{-5}	5.611×10^{-5}
	52	0.15	6.506×10^{-3}	7.146×10^{-3}	7.187×10^{-3}
	52	0.25	3.106×10^{-2}	3.179×10^{-2}	3.233×10^{-2}
	52	0.50	2.760×10^{-1}	2.328×10^{-1}	2.491×10^{-1}
	52	1.00	2.290	1.212	1.441
	165	0.03	1.621×10^{-4}	1.775×10^{-4}	1.775×10^{-4}
	165	0.15	2.064×10^{-2}	2.217×10^{-2}	2.230×10^{-2}
	165	0.25	9.854×10^{-2}	1.028×10^{-1}	1.043×10^{-1}
	165	0.50	8.758×10^{-1}	6.788×10^{-1}	7.167×10^{-1}

^a Size parameter = $\pi d_p/\lambda$. ^b Independ-LM represents the product of the number of primary spheres time the absorption cross section of a primary sphere computed from Lorenz-Mie theory.

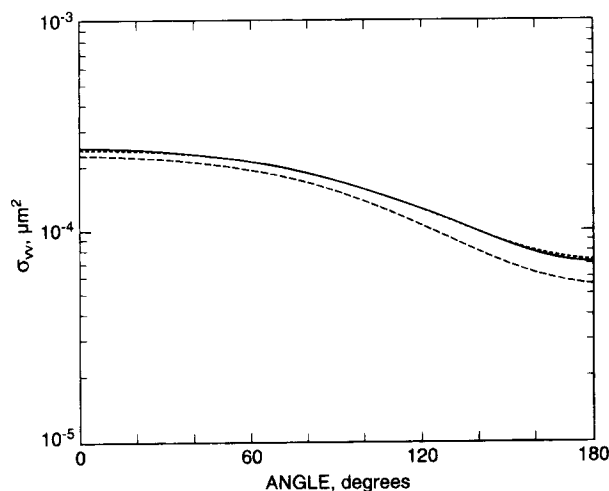


Figure 12. Differential scattering for σ_w for 17 spheres with $n = 1.7 + 0.7i$ and $x = 0.25$ (CEMD solid, CED short dash, RD long dash).

agglomerates by the difference between the CED and CEMD of 25% at small angles. The discrepancy caused by the increasing primary sphere size does not decrease with cluster size (52 spheres in Figure 15). Again there is fair qualitative agreement between the peaks in the various scattering plots though the difference at any one angle may be as much of a factor of 10 for RD versus CEMD and a factor of 2 for CED versus CEMD.

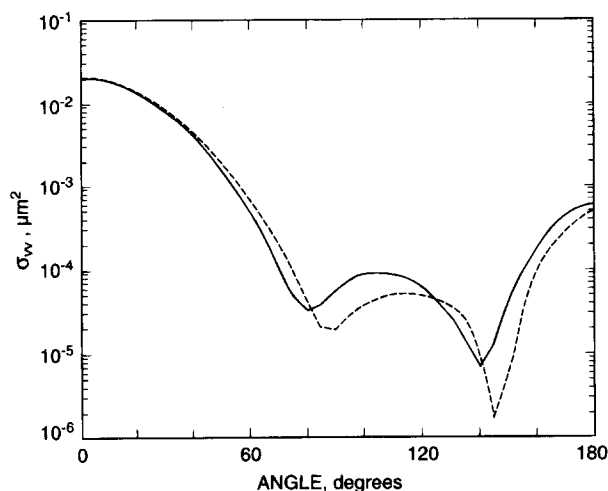


Figure 13. Differential scattering for σ_w 165 spheres with $n = 1.7 + 0.7i$ and $x = 0.25$ (CEMD solid, CED short dash, RD long dash). The CEMD and CED curves are identical.

The polarization ratio, σ^{hh}/σ_w , is plotted in Figures 16 and 17 for agglomerates with 17 and 52 primary spheres for $x = 1.0$. In the Rayleigh-Debye theory this ratio would be simply $\cos \theta$ independent of primary size and agglomerate size. The CEMD results have a minimum value of about 10^{-2} for θ near 90° for both the 17 and 52 sphere agglomerate compared to a value of 0 at 90° for the RD results. The fair agreement between the CEMD result

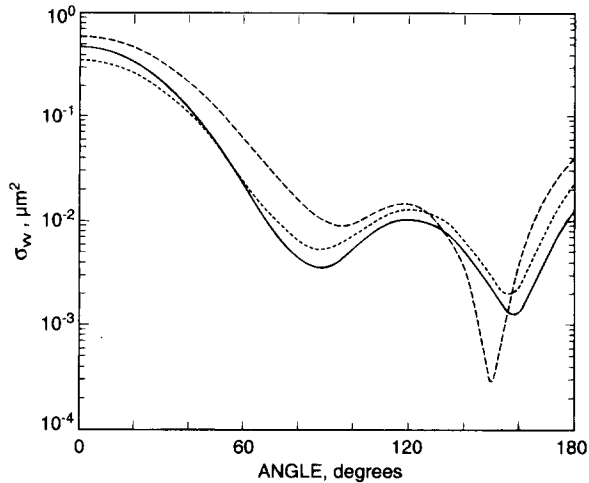


Figure 14. Differential scattering for σ_{vv} for 17 spheres with $n = 1.7 + 0.7i$ and $x = 1.0$ (CEMD solid, CED short dash, RD long dash).

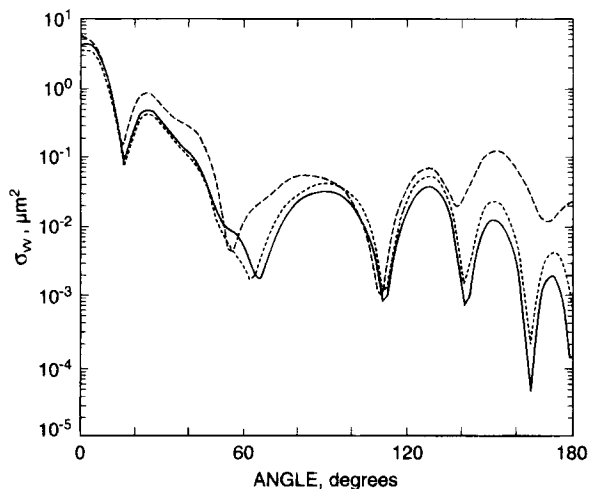


Figure 15. Differential scattering for σ_{vv} for 52 spheres with $n = 1.7 + 0.7i$ and $x = 1.0$ (CEMD solid, CED short dash, RD long dash).

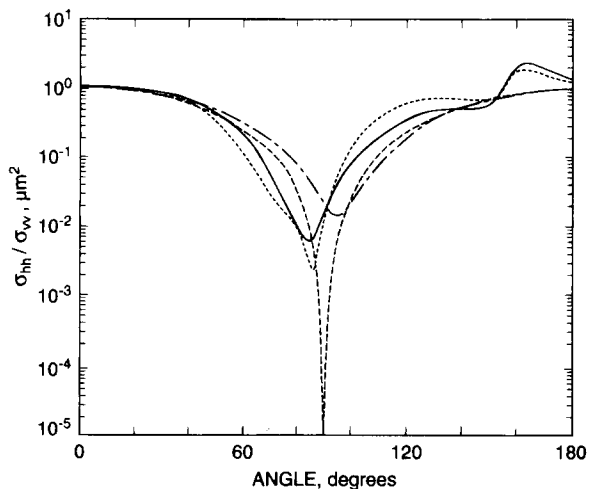


Figure 16. Polarization ratio for 17 spheres with $n = 1.7 + 0.7i$ and $x = 1.0$ (CEMD solid, CED short dash, LM for single sphere alternating long and short dashes, RD long dash).

and the single sphere LM theory results suggests that the polarization ratio near 90° may be determined mainly by the primary sphere size and weakly dependent on the agglomerate size. This could have important implications for characterizing agglomerates from light scattering

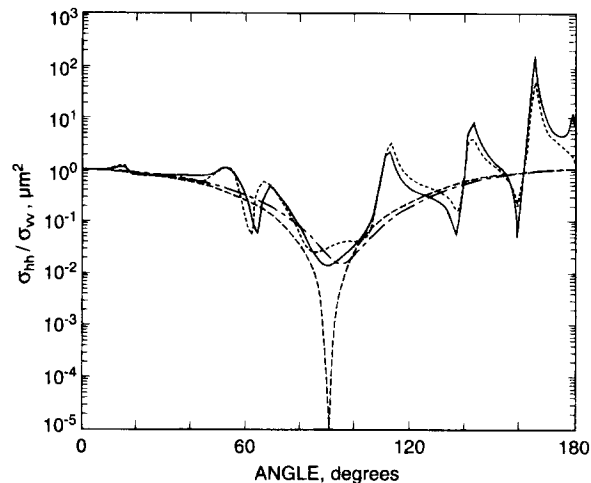


Figure 17. Polarization ratio for 52 spheres with $n = 1.7 + 0.7i$ and $x = 1.0$ (CEMD solid, CED short dash, LM for single sphere alternating long and short dashes, RD long dash).

measurements. The appearance of resonance-like features for the CEMD for the larger agglomerate was not expected. The spiked peaks in the backscatter direction correspond to the spiked minima in σ_{vv} shown in Figure 15. Such features may not be apparent for an orientation average of the scattering function. Another qualitative difference between CEMD and RD is finite depolarized scattering for CEMD compared to none for RD.

Small-Angle Scattering. Small-angle scattering is important for two reasons: in the Rayleigh–Debye approximation, the radius of gyration of the agglomerate can be computed from the small-angle scattering and the square of the number of primary spheres in an agglomerate can be computed from the scattering at $\theta = 0^\circ$.

$$\sigma_{vv}(q) = \sigma_{vv}(q=0)(1 - q^2 R_g^{1q}) \quad (60)$$

$$\sigma_{vv}(q=0) = \frac{k^4 N^2}{16\pi^2} |\alpha_E|^2 \quad (61)$$

Equation 60 is equivalent to eq 57 for the magnetic polarizability, α_H , set equal to 0. Assuming the polarization direction to be along the y axis and light propagation along the z axis, then the xz plane is the vv scattering plane. From eq 56 we find that the $\bar{q} \rightarrow 0$ direction corresponds to the direction of the x axis. The x projection of the radius of gyration is computed using eq 60. The value of q is obtained by trial and error as the value for which σ_{vv} has dropped 10% from its value at $q = 0$. This method is used for RD, CED, and CEMD methods for selected agglomerate sizes and primary sphere sizes for sootlike agglomerates and silica-like agglomerates. We find that in every case the RD result agreed to within 5% with the x projection of the radius of gyration using eq 56 with the coordinates given in Table 4. As indicated in Table 4, the value of R_g^x computed by RD theory agrees within 5% with the CEMD and CED values for the 165 sphere agglomerate for all primary size parameters ≤ 0.5 . For the smaller agglomerates there are differences in the range $\pm 20\%$ depending on the agglomerate size and primary sphere size. The coupled dipole methods seem to overestimate R_g^x for small primary sphere size and underestimate it for large primary sphere size. The same general trends are observed for the silica type agglomerates.

The forward scattering cross section ($q = 0$) computed by RD underestimates the coupled dipole results for small primary sphere and overestimates it for large primary

Table 4. Comparison of R_g^x and $\sigma_{vv}(\theta)$ Computed by RD and the Coupled Dipole Methods for Selected Agglomerates, $\lambda = 0.6328 \mu\text{m}$

x Projection of Radius of Gyration						
refractive index	no. of spheres	size parameter ^a	$R_g^x, \mu\text{m}$			
			RD	CED	CEMD	
1.7 + 0.7	17	0.15	2.45×10^{-2}	2.27×10^{-2}	2.33×10^{-2}	
	17	0.25	3.66×10^{-2}	3.54×10^{-2}	3.66×10^{-2}	
	17	0.50	7.03×10^{-2}	8.10×10^{-2}	8.30×10^{-2}	
	17	1.00	0.142	0.162	0.173	
	52	0.15	9.70×10^{-2}	0.109	0.109	
	52	0.25	0.161	0.189	0.189	
	52	0.50	0.321	0.309	0.308	
	52	1.00	0.643	0.447	0.439	
	165	0.03	1.98×10^{-2}	2.07×10^{-2}	2.07×10^{-2}	
	165	0.15	0.109	0.110	0.110	
	165	0.25	0.183	0.188	0.187	
	165	0.50	0.366	0.374	0.375	
	1.55	52	0.15	9.73×10^{-2}	9.75×10^{-2}	9.76×10^{-2}
		52	0.25	0.162	0.171	0.171
		52	0.50	0.321	0.327	0.326
		52	1.00	0.643	0.505	0.481

Differential Scattering Cross Section for $\theta = 0$						
refractive index	no. of primary spheres	size parameter ^a	$\sigma_{vv}(0), \mu\text{m}^2$			
			RD	CED	CEMD	
1.7 + 0.7i	17	0.03	6.50×10^{-10}	7.06×10^{-10}	7.06×10^{-10}	
	17	0.15	1.03×10^{-5}	1.14×10^{-5}	1.15×10^{-5}	
	17	0.25	2.21×10^{-4}	2.42×10^{-4}	2.47×10^{-4}	
	17	0.50	1.42×10^{-2}	1.24×10^{-2}	1.33×10^{-2}	
	17	1.00	0.591	0.360	0.475	
	52	0.03	6.08×10^{-9}	6.24×10^{-9}	6.24×10^{-9}	
	52	0.15	9.59×10^{-5}	9.88×10^{-5}	9.95×10^{-5}	
	52	0.25	2.07×10^{-3}	2.04×10^{-3}	2.07×10^{-2}	
	52	0.50	0.133	0.113	0.121	
	52	1.00	5.53	3.46	4.25	
	165	0.03	6.12×10^{-8}	6.24×10^{-8}	6.24×10^{-8}	
	165	0.15	9.72×10^{-4}	9.66×10^{-4}	9.76×10^{-4}	
	165	0.25	2.09×10^{-2}	2.06×10^{-2}	2.10×10^{-2}	
	165	0.50	1.34	0.997	1.06	
	1.55	52	0.03	2.02×10^{-9}	2.07×10^{-9}	2.07×10^{-9}
		52	0.15	3.18×10^{-5}	3.35×10^{-5}	3.37×10^{-5}
52		0.25	6.84×10^{-4}	7.26×10^{-3}	7.40×10^{-3}	
52		0.50	0.443	0.461	0.500	
52		1.00	2.59	2.48	3.36	

^a Size parameter = $\pi d_p/\lambda$.

sphere size for sootlike agglomerates, the same as the trend for R_g^x results. For the largest agglomerate, the RD results for the forward scattering cross section agree with the coupled dipole results for primary sphere size parameters ≤ 0.3 . For the nonabsorbing silica-type agglomerate, the coupled dipole result is generally greater than the RD result for forward scattering.

VII. Discussion

The addition of the magnetic dipole term extends the range of the coupled dipole method from a primary sphere size parameter of 0.5 to 1.0 for sootlike doublets. This size parameter range is of interest for UV light scattering by soot generated by laboratory scale fires, which produce primary spheres with diameters in the range 10–50 nm, and to visible light scattering by soot from large fires, which produces primary spheres with diameters as large as 200 nm. One objective of this study was to identify scattering features that could be associated with the primary sphere size independent of the agglomerate size. The polarization ratio at 90° appears to be such a feature. This ratio computed for agglomerates of size 17 and 52 with a primary sphere $x = 1$ is similar in magnitude to the LM prediction for a single primary sphere as shown in Figures 16 and 17. There is a need to obtain the

orientation averaged values for a range of agglomerate sizes to better define the utility of this diagnostic technique.

We find that σ_e computed by CED for the 52 sphere sootlike agglomerate and for the silica-like agglomerate with $x = 1$ differ by 12% and 20%, respectively, from the CEMD result. Ku³⁰ had compared the CED prediction using the Dungey–Bohren²² expression for polarizability for a 136-dipoles pseudosphere with the exact Lorenz–Mie theory prediction. For a range of optical properties, the CED value of the extinction cross section agrees within 10% with the LM solution for $x \leq 1$. So it appears that the range of validity of CED as a function of primary sphere size for the extinction cross section may be larger for compact objects than for agglomerates. It should also be stated that good agreement for the extinction cross section does not imply good agreement for the total scattering cross section or the differential scattering cross section.

The motivation for the CEMD method was that improving the single particle calculation by adding a magnetic dipole term would also improve the calculation of the properties of an agglomerate. An obvious extension is to include the quadrupole moments. There is a possible fly in the ointment. Equations 17 and 18 relate the dipole

moments to a plane incident wave. The exciting fields given in eqs 13 and 15 are not plane waves and their magnitudes vary over the volume of a neighboring sphere. Yet eqs 17 and 18 are also used for the exciting field and this makes the analysis approximate. So while we think it is likely that including the quadrupole and higher order terms will be an improvement, there is still a need to check with an exact solution. For the larger primary sphere sizes it is likely that the successive approximation used in solving eqs 32 and 33 will not converge so that an alternative solution method such as the conjugate gradient technique will be needed.

The RD method is of great value because it provides a direct link between agglomerate structure and scattering measurements. Consequently it is of great interest to know its limitations. Our study indicates that for size parameter ≤ 0.25 the RD method is valid for large agglomerates. For small agglomerates in certain orientations, there can be up to a 30% difference between the coupled dipole and RD results.

One might expect the coupled methods to reduce to the RD method in the limit of small particle size. This is not the case for two small spheres in contact. As shown in Table 1 the coupling field is 11% of the incident field for the broadside incidence orientation for a size parameter of 0.1; it remains at 11% for smaller primary sphere sizes. The reason is that the inverse dependence of the exciting field with r^3 (eq 15) is compensated by the x^3 dependence of a_1 for small x . The presence of the exciting field increases the scattering cross section by 25% for the broadside orientation and decreases it by 11% for the end-on orientation. For five spheres in a linear array with size parameter 0.1142, Fuller³¹ obtained a 27% enhancement of the orientation averaged total scattering cross section relative to the RD prediction.

As the agglomerate size increases, the difference between the RD and the coupled dipole calculations diminishes. With increasing size, the strong orientation effects for small clusters are apparently averaged out.

The differences diminish systematically from a two-sphere cluster to an agglomerate with 165 primary spheres for total scattering and small angle scattering. However, there is a large difference in the scattering intensity for RD and CEMD around 150° as indicated in Figure 13. Singham and Bohren,¹¹ on the other hand, indicate differences less than 5% between the RD results and the CED results for all angles. As expected the differences obtained for a single orientation calculation are much greater than an orientation averaged result such as obtained by Singham and Bohren. For silica-like agglomerates, there are larger deviations between RD and CEMD with about a 10% difference in the total scattering cross section for $N = 165$, $x = 0.25$ compared to a 1% difference for the sootlike agglomerate. The absorption cross section computed for sootlike agglomerates for size parameter ≤ 0.25 by CED and CEMD is greater than by RD, where by RD we mean the independent particle approximation of N times the absorption cross section of a single sphere computed by LM Theory. This is in qualitative agreement with Nelson's⁸ results for agglomerates with up to 50 primary spheres and Iskander *et al.*⁹ with up to 164 primary spheres. We do not see the resonance effect at small primary sphere sizes reported by Iskander. Also for $x > 0.3$, there is a decrease in the absorption relative to RD as a result of shielding. This effect is seen by Iskander for refractive index $2 + i$, $N = 164$, at $x = 0.5$.

Acknowledgment. Raymond Mountain at NIST generated the agglomerates by a Brownian dynamics computer simulation. Craig Bohren is supported by the National Science Foundation under Grant No. ATM-8810876, Kirk Fuller by National Park Service Grant No. NA90RAH000077, and George Mulholland by Life Sciences Division of National Aeronautics and Space Administration under Grant No. W-17980 and by The Pennsylvania State University Particulate Materials Center while on sabbatical leave at Penn State. George Mulholland thanks Robert Santoro and Gary Messing for their hospitality during his sabbatical at Penn State.

(31) Fuller, K. A. Submitted to *Appl. Opt.*